Journal of Materials Chemistry A

ROYAL SOCIETY OF CHEMISTRY

PAPER

View Article Online
View Journal | View Issue

Check for updates

Cite this: J. Mater. Chem. A, 2020, 8, 19502

Lithiation of $V_2O_3(SO_4)_2$ – a flexible insertion host†

Stephanie F. Linnell, [a] Julia L. Payne, [a] David M. Pickup,[b] Alan V. Chadwick,[b] A. Robert Armstong [a] and John T. S. Irvine *[a]

Received 6th July 2020
Accepted 9th September 2020

DOI: 10.1039/d0ta06608g

rsc.li/materials-a

Materials that display strong capabilities for lithium insertion without significant change in unit cell size on cycling are of considerable importance for electrochemical applications. Here, we present $V_2O_3(SO_4)_2$ as a host for lithium-ion batteries. Electrochemically, 2.0 Li^+ ions can be inserted, giving $Li_2V_2O_3(SO_4)_2$ with an oxidation state of V^{4+}, as determined by X-ray absorption spectroscopy. The capacity of $V_2O_3(SO_4)_2$ can be increased from 157 mA h g^{-1} to 313 mA h g^{-1} with the insertion of two additional Li^+ ions which would drastically improve the energy density of this material, but this would be over a wider potential range. Chemical lithiation using *n*-butyllithium was performed and characterisation using a range of techniques showed that a composition of $Li_4V_2O_3(SO_4)_2$ can be obtained with an oxidation state of V^{3+}. Structural studies of the lithiated materials by X-ray diffraction showed that up to 4.0 Li^+ ions can be inserted into $V_2O_3(SO_4)_2$ whilst maintaining its framework structure.

Open Access Article. Published on 10 September 2020. Downloaded on 12/6/2025 8:19:50 AM. This article is licensed under a Creative Commons Attribution 3.0 Unported Licence.

Introduction

Materials that can reversibly incorporate large numbers of ions balanced by redox changes in the host lattice are a subject of much interest, with important applications such as electrochromics and battery electrodes. One such application is in the search for less expensive positive electrode materials for high energy density lithium-ion batteries (LIBs). Consequently, great efforts have been devoted to the search for crystal structures that allow a large amount of lithium storage at high redox potentials but remain structurally stable on cycling.[1] Polyanion compounds (phosphates, sulfates) are promising candidates due to their structural stability and higher operating potentials compared to oxides.[2,3] Among them $LiFePO_4$ has been extensively studied and commercialised, but its energy density (~580 W h kg^{-1}) is limited due to its relatively low operating voltage of 3.45 V *vs.* Li^+/Li^0.[4,5] Tavorite-structured compounds including $LiFeSO_4F$,[6,7] $LiVPO_4F$,[8–12] and $LiVPO_4O$,[13–15] operate at higher voltages, are structurally stable and are considered attractive alternatives. In particular, the vanadium based materials have attracted considerable interest, due to the ability to adopt a range of oxidation states, 2+, 3+, 4+ and 5+, enabling them to insert/extract reversibly-more than one Li^+ ion per transition metal ion. The Li^+ extraction/insertion in $LiVPO_4F$ is associated with two redox processes and when the two reactions are utilised this material can achieve a specific capacity of 312 mA h g^{-1}. The insertion of Li^+ occurs at 1.80 V *vs.* Li^+/Li^0 and is associated with the V^{3+}/V^{2+} redox couple and extraction of Li^+ occurs *via* two plateaux at 4.24 V and 4.28 V *vs.* Li^+/Li^0 associated with the V^{4+}/V^{3+} redox couple.[12] Structural studies have revealed shifts from the triclinic $LiVPO_4F$ pristine phase to monoclinic Li_2VPO_4F and VPO_4F phases along with unit cell volume expansions/contractions but with retention of the VPO_4F framework on cycling.[12] As for $LiVPO_4O$, this material can also exploit two redox couples and thereby deliver a specific capacity of 318 mA h g^{-1}.[12] The insertion of Li^+ is associated with the V^{3+}/V^{4+} redox couple, with three short plateaux at 2.45 V, 2.21 V and 2.04 V attributed to the formation of $Li_{1.5}VPO_4O$, $Li_{1.75}VPO_4O$ and Li_2VPO_4O, respectively. Over the higher voltage range, Li^+ is extracted with one plateau observed at 3.95 V associated with the V^{4+}/V^{5+} redox couple and the formation of ε-VPO_4O.[13] The Li_xVPO_4O ($0 < x < 2$) phases can be indexed to different space groups, showing unit cell volume expansions/contractions and the VPO_4O framework is maintained on cycling *vs.* Li^+/Li^0 with changes in the V–O bond distances for the different phases, due to the formation of the V=O bond within the VO_6 octahedra for the V^{4+} and V^{5+} phases, which is absent for the V^{3+} phase.[13]

Other materials of interest include the vanadyl phosphate, $Li_4VO(PO_4)_2$. This material operates at a relatively high voltage of 4.1 V *vs.* Li^+/Li^0 and exhibits a reversible capacity of 70 mA h g^{-1} which is associated with the V^{4+}/V^{5+} redox couple.[16,17] The PO_4^{3-} polyanion in $Li_4VO(PO_4)_2$ has been replaced with the more electronegative SO_4^{2-} polyanion to give $Li_2VO(SO_4)_2$.[18] $Li_2VO(SO_4)_2$ shows a plateau at 4.7 V *vs.* Li^+/Li^0 associated with the V^{5+}/V^{4+} redox couple and delivers a reversible capacity of 50 mA h g^{-1}.[18] Despite reaching a higher potential, vanadium-based materials that utilise the SO_4^{2-} polyanion remain underexplored.[18–21] Vanadium sulfates are attractive candidate compounds and while the search for new

[a]School of Chemistry, University of St Andrews, St Andrews, Fife, KY16 9ST, UK. E-mail: jtsi@st-andrews.ac.uk

[b]School of Physical Science, University of Kent, Canterbury, CT2 7NH, UK

† Electronic supplementary information (ESI) available: More Rietveld refinements and Rietveld refinement results, additional electrochemical data, and EXAFS analysis. See DOI: 10.1039/d0ta06608g

This journal is © The Royal Society of Chemistry 2020

Open Access Article. Published on 10 September 2020. Downloaded on 12/6/2025 8:19:50 AM. This article is licensed under a Creative Commons Attribution 3.0 Unported Licence.

crystal structures and compositions is ongoing, there are existing vanadium sulfates that can be explored.[18,22]

$V_2O_3(SO_4)_2$ can accept four Li^+ ions, delivering a theoretical capacity of 313 mA h g^{-1}. Here, we study the Li^+ insertion into $V_2O_3(SO_4)_2$ using two methods (1) electrochemical lithiation and (2) chemical lithiation using *n*-butyllithium. $V_2O_3(SO_4)_2$ positive electrodes were cycled in Swagelok-type cells between 4.20 V and 1.95 V *vs.* Li^+/Li^0 and examined *ex situ* by means of X-ray absorption spectroscopy, infrared spectroscopy and powder Xray diffraction studies to reveal the phase evolution and structural changes which occur at different stages during the lithiation and delithiation process. $V_2O_3(SO_4)_2$ was also chemically lithiated to insert two additional Li^+ ions. X-ray diffraction studies, inductively coupled plasma optical emission spectroscopy analysis and X-ray absorption spectroscopy measurements were carried out to understand the structural evolution accompanying the chemical insertion of Li^+ ions.

Experimental

Synthesis of $V_2O_3(SO_4)_2$

$V_2O_3(SO_4)_2$ was synthesised by modifying a method reported by Richter *et al.*[23] V_2O_5 (Sigma Aldrich, ≥99.6%, 3.64 g) was stirred with an excess of concentrated sulfuric acid (Fischer, >95%, 30 mL) at 140 °C for 48 h according to eqn (1).

$$V_2O_5 + 2H_2SO_4 \rightarrow V_2O_3(SO_4)_2 + 2H_2O \quad (1)$$

Once cooled, the product was filtered under vacuum and washed with cold concentrated H_2SO_4, followed by a further washing with CF_3COOH (Alfa Aesar, 99%) and finally dried at 200 °C overnight. The product was stored and handled in an argon filled glovebox due to its hygroscopicity.

Electrochemical lithiation

Electrodes were prepared by ball-milling 80 wt% active material with 20 wt% carbon super C65 (Imerys) at 300 rpm under argon for 30 min. A Fritsch Pulverisette planetary ball mill was used with 10 mm diameter zirconia milling balls. Electrochemical tests of the $V_2O_3(SO_4)_2$ positive electrodes were performed in Swagelok type cells which were assembled in an argon filled glovebox. Positive electrodes were separated from the Li metal disc negative electrode by a Whatman GF/D borosilicate glass fibre sheet saturated with 1 M $LiPF_6$ in ethylene carbonate/dimethyl carbonate [1 : 1 (w/w)] (LP30, BASF) as the electrolyte. In order to evaluate the electrochemical lithiation of $V_2O_3(SO_4)_2$ as a positive electrode, cells were cycled in a temperature-controlled environment at 30 °C using a Mac Pile Bio Logic II system in galvanostatic mode. To determine the cycling performance a cell was cycled over different rates (C/20, C/10, C/5, C/2 and C) at 30 °C using a Maccor Series 4200 system.

To understand the Li^+ insertion/extraction in $V_2O_3(SO_4)_2$, multiple cells were discharged at a rate of C/20 to various states of discharge and charge. The positive electrodes were recovered from the $V_2O_3(SO_4)_2$||Li cells after cycling, washed with dimethyl carbonate (DMC, Sigma Aldrich, ≥99%) three times in an argon filled glovebox, and dried under vacuum overnight.

Chemical lithiation

Four chemical lithiation reactions were performed with *n*-butyllithium (1.6 M in hexanes, Sigma Aldrich) in an argon filled glovebox at room temperature. $V_2O_3(SO_4)_2$ (1.46 mmol) was dispersed in *n*-hexanes (Sigma Aldrich, 95%, ≤20 mL) and four different amounts of *n*-butyllithium were added, as detailed in Table 1. The dispersions were stirred continuously for two weeks. The products were filtered, washed with *n*-hexanes, dried under vacuum and handled in an argon filled glovebox.

Materials characterisation

The pristine phase, $V_2O_3(SO_4)_2$, and lithiated samples were examined using inductively coupled plasma optical emission spectroscopy (ICP-OES) analysis, powder X-ray diffraction (PXRD), neutron powder diffraction (NPD), X-ray absorption spectroscopy (XAS) and infrared (IR) spectroscopy, optical microscopy and scanning electron microscopy (SEM).

ICP-OES analysis was performed on the chemically lithiated samples using a Thermo Fisher Scientific ICP-OES iCAP 6000. Standards were prepared for lithium by diluting concentrated commercial ICP-OES standards to four different concentrations. The chemically lithiated samples were dissolved using aqua regia (solution of nitric acid and hydrochloric acid at a 1 : 3 ratio by volume).

Laboratory PXRD patterns were collected on a PANanalytical Empyrean diffractometer, using Mo-K$\alpha_{1,2}$ radiation ($\lambda = 0.7107$ Å) with a Zr β-filter and X'celerator detector. Data were collected in the 2θ range, 3.5–35.0° over 16 h per scan with a step size of 0.0167°, in capillaries at room temperature. Samples were loaded into glass capillaries (0.7 mm diameter) in an argon filled glovebox. An NPD pattern was obtained on the GEM diffractometer at the ISIS Neutron and Muon Source, UK. The powdered sample was loaded into a 8 mm vanadium can under argon and sealed using an indium wire and the measurement was made under ambient conditions over 1 h. Diffraction data were analysed using the Rietveld method using the general structural analysis system (GSAS) and its associated graphical user interface program (EXPGUI).[24,25]

Vanadium K-edge (5.4651 keV) X-ray absorption spectra were acquired in transmission on B18 beamline at Diamond Light Source, UK. The powdered samples (8 mg of active material)

Table 1 Summary of the chemical lithiation reactions

		n-Butyllithium	
$V_2O_3(SO_4)_2$/mmol	*n*-Hexane/mL	Moles/mmol	Volume/mL
1.46	10	1.46	0.91
1.46	10	2.92	1.83
1.46	20	5.85	3.65
1.46	20	11.70	7.30

Open Access Article. Published on 10 September 2020. Downloaded on 12/6/2025 8:19:50 AM.
This article is licensed under a Creative Commons Attribution 3.0 Unported Licence.

were ground for 30 min with cellulose (150 mg) and pressed into 13 mm diameter pellets, and then sealed into aluminium bags in an argon filled glovebox. XAS spectra of the vanadium metal foil were acquired simultaneously with the experimental samples. All spectra were acquired in triplicate for each sample. XAS spectra were aligned, merged and normalised using the software program Athena and EXAFS spectra were fitted using the program Artemis.[26,27]

An IRAffinity-1 Shimadzu Fourier transform IR spectrometer was used to obtain IR spectra. The powdered samples were placed directly onto the diamond crystal and IR spectra collected at room temperature between 4000 and 400 cm^{-1}. Optical microscopy images were collected using a Meiji Techno microscope fitted with a Canon PowerShot G6 digital camera. A JEOL JSM-5600 SEM fitted with a tungsten filament electron source and a secondary electron detector were used to examine the morphology of the samples.

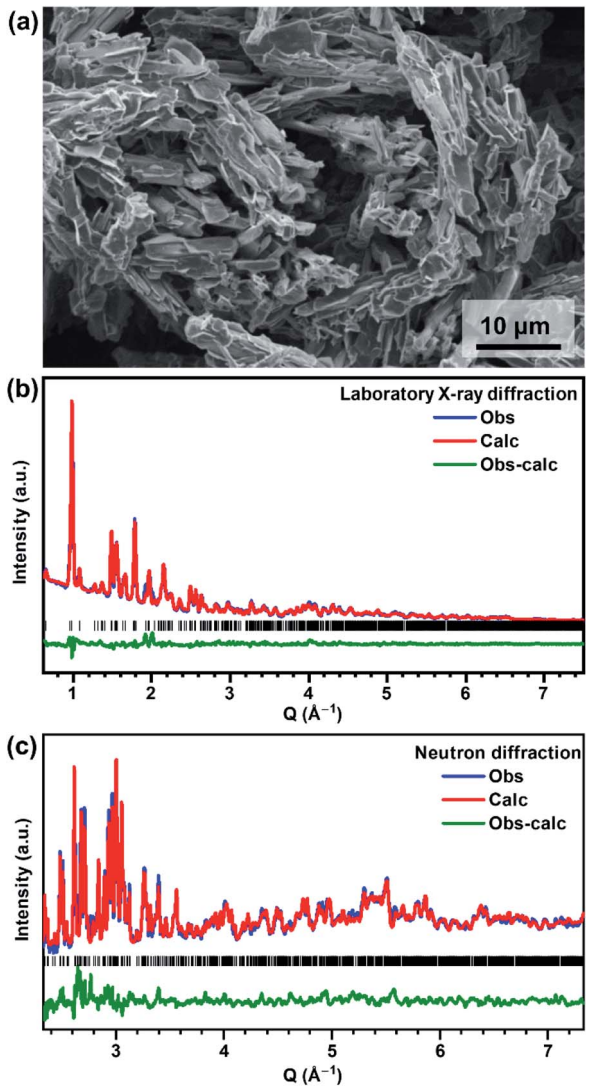

Fig. 1 (a) SEM micrograph of $V_2O_3(SO_4)_2$, (b) laboratory X-ray diffraction Rietveld fit and (c) neutron diffraction Rietveld fit for $V_2O_3(SO_4)_2$ using the structural model published by Richter *et al.* as the starting model.[23]

Results and discussion

Characterisation of $V_2O_3(SO_4)_2$

$V_2O_3(SO_4)_2$ was successfully prepared using a lower temperature of 140 °C, compared to the previously reported synthesis temperature of 180 °C.[23] The SEM micrograph of $V_2O_3(SO_4)_2$, shown in Fig. 1(a) reveals a homogeneous morphology consisting of acicular crystallites.

$V_2O_3(SO_4)_2$ can be indexed to a monoclinic unit cell with the space group $P2_1/a$ and unit cell parameters $a = 9.464(12)$ Å, $b = 8.908(13)$ Å, $c = 9.939(12)$ Å, $\beta = 104.732(4)$ °. All peaks were indexed and the unit cell parameters correspond well with those reported by Richter *et al.*[23] A Rietveld refinement was performed using the structural model published by Richter *et al.*[23] The Rietveld fits of the PXRD and NPD data are shown in Fig. 1(b) and (c), respectively, and the atomic coordinates and isotropic thermal parameters are given in the ESI, Table S1.†

The structure of $V_2O_3(SO_4)_2$ is illustrated in Fig. 2. $V_2O_3(SO_4)_2$ is made up of pairs of vanadium octahedra linked by a bridging oxygen atom and two corner-sharing SO_4 tetrahedra, forming

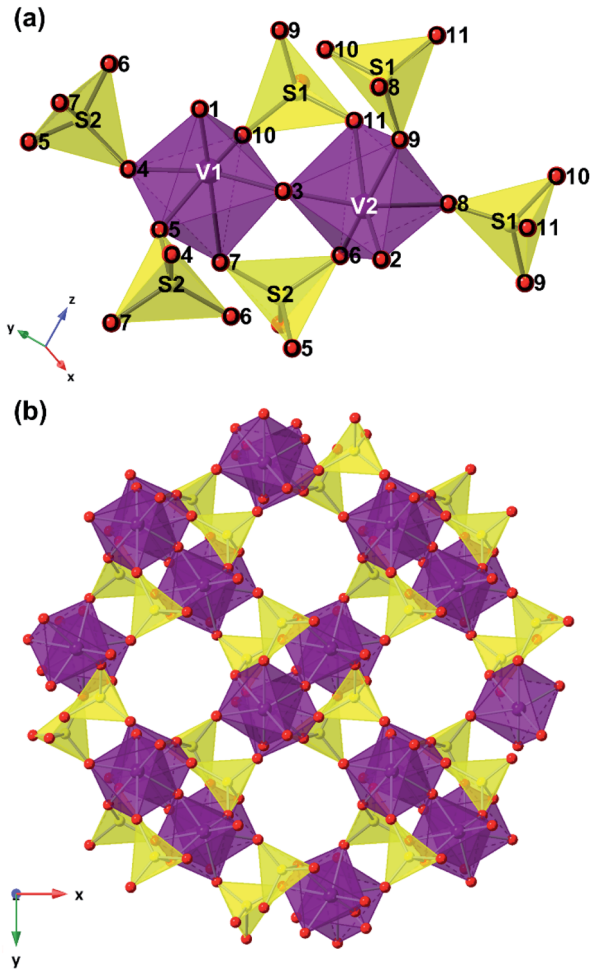

Fig. 2 Structural model of $V_2O_3(SO_4)_2$ showing (a) the $[V_2O_3]^{4+}$ subunit made up of pairs of vanadium octahedra (purple polyhedra) linked to each other by a bridging oxygen atom (red spheres) and two bridging SO_4 tetrahedra (yellow polyhedra) and (b) the open channels down the *c*-axis.

This journal is © The Royal Society of Chemistry 2020

Open Access Article. Published on 10 September 2020. Downloaded on 12/6/2025 8:19:50 AM.
This article is licensed under a Creative Commons Attribution 3.0 Unported Licence.

the $[V_2O_3]^{4+}$ subunit which consists of the two species, $[V(1)O_2]^+$ and $[V(2)O]^{3+}$, as shown in Fig. 2(a). The corner sharing VO_6 distorted octahedra and SO_4 tetrahedra create a three-dimensional network with open channels running down the *c* axis as illustrated in Fig. 2(b). The VO bond lengths in $V_2O_3(SO_4)_2$ are summarised in Table S2.†

Electrochemical lithiation

The electrochemical Li^+ insertion/extraction process in $V_2O_3(SO_4)_2$ was explored. Cells were cycled in galvanostatic mode between 4.20 V and 1.95 V at a rate of C/20, starting on discharge. The galvanostatic discharge–charge curves for the first, second, third and fifth cycles and the derivative d*x*/d*V* curve of the first cycle are shown in Fig. 3(a) and (b), respectively. The galvanostatic curve (Fig. 3(a)) reveals four sloping plateaux on discharge and charge, and approximately 2.0 Li^+ (160 mA h g^{-1}) were inserted on the first discharge, hence the average vanadium oxidation state reached +4.00. The d*x*/d*V* curve (Fig. 3(b)) shows four redox peaks centred about 4.09 V, 3.25 V, 2.83 V and 2.23 V *vs.* Li^+/Li^0. The intensities of the reduction peaks are greater than those of the oxidation peaks, suggesting that not all the Li^+ that was inserted could be extracted. As for the redox processes centred about 3.25 V, the d*x*/d*V* curve shows two reduction peaks at 3.23 V and 3.14 V and two oxidation peaks at 3.15 V and 3.11 V. These peaks suggest charge-ordering of the vanadium atoms or vacancy-ordering of Li^+ which has been reported for $Li_xMn_2O_4$ among other systems.[28–30] Upon subsequent cycling, the electrode can reversibly insert approximately 1.5 Li^+, leading to a reversible capacity of approximately 120 mA h g^{-1}, which progressively decays upon cycling. Additionally, a cell was cycled in potentiostatic mode at a slow rate of 5.6 μV s^{-1} between 4.20 V and 1.95 V. The voltammogram is shown in Fig. S1† and corresponds well with the d*x*/d*V* curve obtained from galvanostatic cycling (Fig. 3(b)), showing the same four redox processes occurring at 4.09 V, 3.25 V, 2.83 V and 2.23 V *vs.* Li^+/Li^0.

Fig. 3(c) shows the specific capacities over different C-rates (C/20, C/10, C/5, C/2 and C). The first cycle at C/20 shows some irreversible capacity (coulombic efficiency of 90%) but subsequent cycles at C/20 show a lower capacity but greater coulombic efficiency of 97%. The discharge and charge capacities decreased to 25 mA h g^{-1} at 1C. After cycling at the faster C-rates a reasonable capacity (110 mA h g^{-1}, coulombic efficiency of 92%) was reached by the 27th cycle at C/20, suggesting that $V_2O_3(SO_4)_2$ did not degrade after cycling at faster rates. The first cycle of each C-rate shows greater irreversible capacity than the subsequent cycles, indicating that the redox processes are rate dependent.

To understand the electrochemical Li^+ insertion/extraction in $V_2O_3(SO_4)_2$ multiple cells of $V_2O_3(SO_4)_2$||Li were discharged to the potentials 3.50 V, 2.95 V, 2.40 V and 1.95 V and charged to 4.00 V. These potentials were selected because they correspond to the inflection points observed between the plateaux in the voltage profile and d*x*/d*V* curves (Figure S2†).

Chemical lithiation

ICP-OES data were collected to determine the amount of lithium in the chemically lithiated samples and their

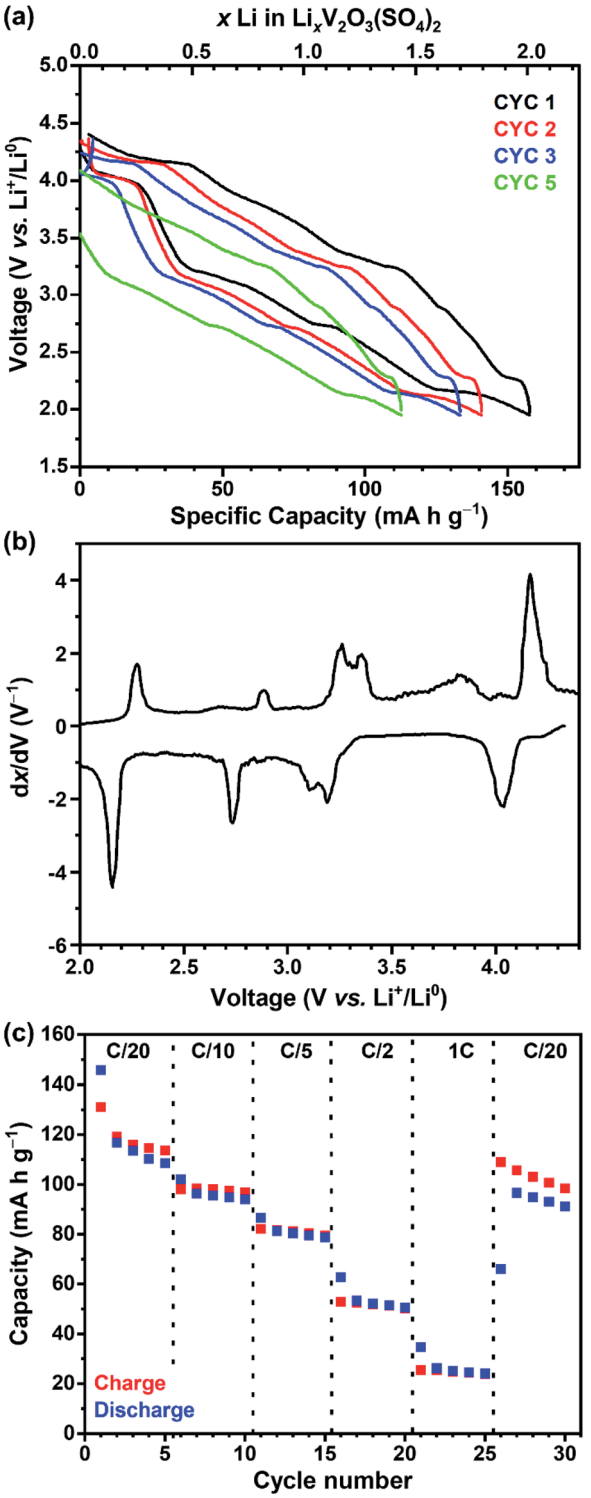

Fig. 3 (a) $V_2O_3(SO_4)_2$||Li cell cycled at a rate of C/20 between 4.20 V and 1.95 V showing the voltage–capacity curve for the first (black), second (red), third (blue) and fifth cycles (green), (b) the derivative d*x*/d*V* curve of the first cycle and (c) the specific capacity *versus* different C-rates (C/20, C/10, C/5, C/2, 1C) of $V_2O_3(SO_4)_2$ cycled between 4.20 V and 1.95 V *vs.* Li^+/Li^0.

Open Access Article. Published on 10 September 2020. Downloaded on 12/6/2025 8:19:50 AM.
This article is licensed under a Creative Commons Attribution 3.0 Unported Licence.

Table 2 Lithium content in the chemically lithiated samples obtained from ICP-OES analysis

Moles of *n*-butyllithium/mol	*x* Li from ICP-OES analysis	Experimental composition	Vanadium oxidation state based on composition
0.00	0.00(0)	$V_2O_3(SO_4)_2$	+5.00(0)
1.46	0.97(2)	$Li_{0.97}V_2O_3(SO_4)_2$	+4.52(1)
2.92	1.64(16)	$Li_{1.64}V_2O_3(SO_4)_2$	+4.18(8)
5.85	2.47(3)	$Li_{2.47}V_2O_3(SO_4)_2$	+3.77(2)
11.70	3.97(5)	$Li_{3.97}V_2O_3(SO_4)_2$	+3.02(3)

compositions are given in Table 2. The oxidation states of vanadium are also given in Table 2. These were calculated based on charge balance considerations, assuming the oxidation states of lithium and oxygen are +1 and −2, respectively, and that all the lithium present in the sample was incorporated into $V_2O_3(SO_4)_2$.

Chemical lithiation of $V_2O_3(SO_4)_2$ resulted in colour changes as shown in Fig. 4, from the yellow pristine phase, $V_2O_3(SO_4)_2$, to green $Li_{0.97}V_2O_3(SO_4)_2$, darker green $Li_{1.64}V_2O_3(SO_4)_2$ and $Li_{2.47}V_2O_3(SO_4)_2$, to dark blue $Li_{3.97}V_2O_3(SO_4)_2$. Optical images, also presented in Fig. 4, show the samples getting darker in colour with increasing Li^+ content. These colour changes are consistent with changes in the vanadium oxidation state as discussed below. SEM micrographs of the chemically lithiated samples, shown in Fig. 4, show some needle-shaped crystallites which are consistent with $V_2O_3(SO_4)_2$ (Fig. 1(a)), suggesting that Li^+ insertion did not cause the morphology of $V_2O_3(SO_4)_2$ to break down completely.

Vanadium oxidation state of $Li_xV_2O_3(SO_4)_2$

To confirm that the Li^+ insertion was accompanied by a change in the vanadium oxidation state, vanadium K-edge XAS measurements were performed. Data were collected on $V_2O_3(SO_4)_2$ electrodes at various states of discharge and charge, the chemically lithiated phases, as well as vanadium foil, V_2O_3, $VOSO_4 \cdot 3H_2O$ and V_2O_5 reference compounds with vanadium formal oxidation states of 0, +3, +4, and +5, respectively. The XANES spectra for V_2O_5, $VOSO_4 \cdot 3H_2O$ and V_2O_3 reference compounds, the pristine phase, $V_2O_3(SO_4)_2$ and the electrochemically lithiated samples are compared in Fig. 5(a) and the chemically lithiated samples are shown in Fig. 5(b).

Fig. 5(a) and (b) show the intensity of the pre-edge peak decreases with increasing Li^+ content. The intensity of the pre-edge peak is correlated to the size of the VO_x coordination sphere which is 55% of the total intensity.[31] This suggests that the shorter, vanadyl V=O bonds increase in length and thereby the VO_6 octahedra become more symmetrical.

This is consistent with a V^{5+} to V^{4+} transition for the electrode discharged to 1.95 V and a transition to V^{3+} for $Li_{3.97}V_2O_3(SO_4)_2$.[31,32]

Furthermore, Fig. 5(a) and (b) reveal a small difference in the edge energies for V_2O_5 and $V_2O_3(SO_4)_2$, despite these materials having the same oxidation state because the edge energy of a material is also influenced by differences in coordination

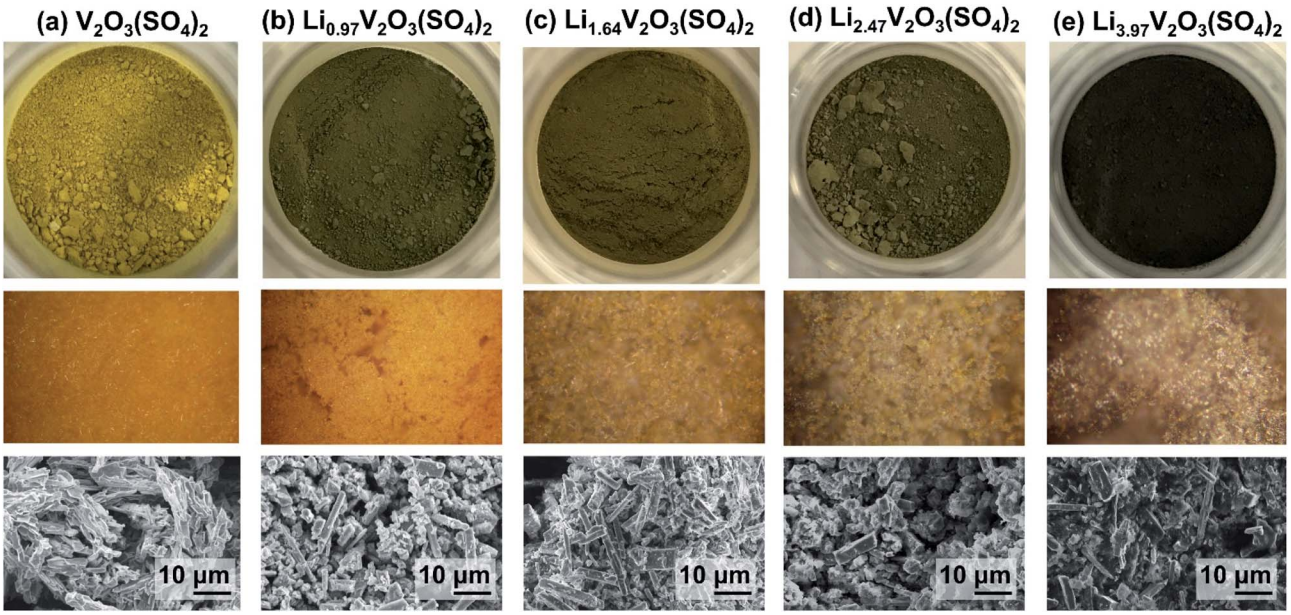

Fig. 4 Photographs (top), optical microscopy images (middle) and SEM micrographs (bottom) showing the colours and morphologies of (a) $V_2O_3(SO_4)_2$, (b) $Li_{0.97}V_2O_3(SO_4)_2$, (c) $Li_{1.64}V_2O_3(SO_4)_2$, (d) $Li_{2.47}V_2O_3(SO_4)_2$ and (e) $Li_{3.97}V_2O_3(SO_4)_2$.

 This journal is © The Royal Society of Chemistry 2020

Open Access Article. Published on 10 September 2020. Downloaded on 12/6/2025 8:19:50 AM.
This article is licensed under a Creative Commons Attribution 3.0 Unported Licence.

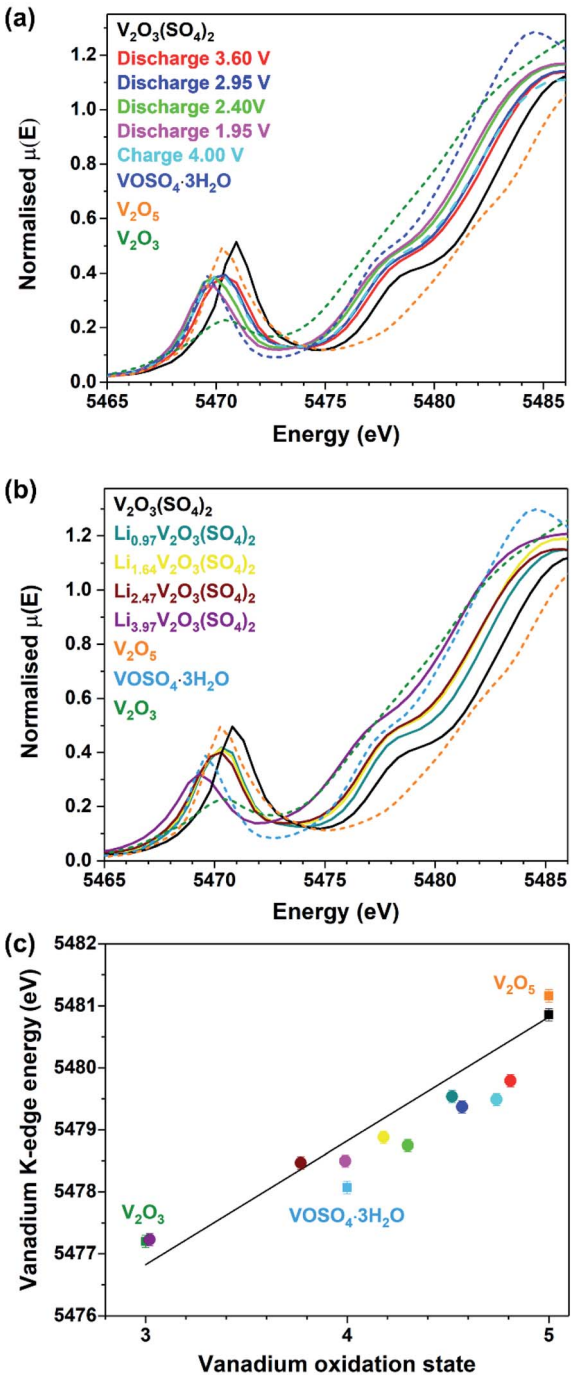

Fig. 5 Vanadium K-edge XANES data showing (a) normalised spectra for the $V_2O_3(SO_4)_2$ electrodes at various states of discharge and charge compared to the reference materials, V_2O_5, $VOSO_4{\cdot}3H_2O$ and V_2O_3, (b) normalised spectra for the chemically lithiated $V_2O_3(SO_4)_2$ samples compared to the reference materials and (c) vanadium K-edge energy (at half-height) as a function of oxidation state.

number and electronegativity of the ligands.[31] The edge positions of the lithiated phases shift progressively to lower energies with increasing Li^+ content relative to $V_2O_3(SO_4)_2$. The edge energy of the $V_2O_3(SO_4)_2$ electrode discharged to 1.95 V is similar to the reference material, $VOSO_4{\cdot}3H_2O$, suggesting that approximately 2.0 mol Li per mol $V_2O_3(SO_4)_2$ were inserted electrochemically, which is in agreement with the electrochemical data (Fig. 3). The edge energy of the $V_2O_3(SO_4)_2$ electrode charged to 4.00 V was shifted to a higher energy relative to the electrode discharged to 1.95 V, suggesting an increase in the vanadium oxidation state upon Li^+ extraction, as expected.[33] However, the electrode charged to 4.00 V shows a similar edge energy to the electrode discharged to 3.60 V, implying that the electrochemical process was partially irreversible.

The edge energies of the chemically lithiated materials also shift to lower energies with increasing Li^+ content, suggesting Li^+ was incorporated into the structure of $V_2O_3(SO_4)_2$ in agreement with the colour changes observed (Fig. 4). $Li_{3.97}V_2O_3(SO_4)_2$ has a very similar edge energy to V_2O_3, implying approximately 4.0 Li^+ per mol was incorporated which agrees with the ICP-OES analysis for this phase. The absorption edge energies for the reference compounds V_2O_3, $VOSO_4{\cdot}3H_2O$, V_2O_5, $V_2O_3(SO_4)_2$ are plotted in Fig. 5(c); these edge energies exhibit an essentially linear relationship with formal oxidation state. The edge energies of the reference materials are similar to those previously reported, thus a comparable linear relationship was obtained.[31,33,34] To determine if the energy shifts of the absorption energies are consistent with the Li^+ content, the energies of the absorption edges taken at half-height of the normalised spectra, were plotted against vanadium oxidation state. The Li^+ content was derived from the electrochemical data for the electrochemically lithiated samples and ICP-OES analysis for the chemically lithiated samples. The average oxidation state of vanadium was calculated from the composition by assuming that the oxidation states of lithium and oxygen were +1 and −2, respectively. The edge energies for the electrochemically lithiated samples suggest that the vanadium oxidation states are comparable to those estimated based on the electrochemical data. Similar edge shifts have also been reported for other vanadium-based electrodes, including for example $Li_xV_2O_5$, $LiVOPO_4$ and $Na_xVPO_{4.8}F_{0.7}$.[14,32,33,35,36] As for $Li_{3.97}V_2O_3(SO_4)_2$, its edge energy shows 4.0 Li^+ per mol of $V_2O_3(SO_4)_2$ were inserted, thereby demonstrating that two additional mol of Li per mol of $V_2O_3(SO_4)_2$ can be inserted chemically.

The experimental compositions and vanadium oxidation states for the lithiated samples are given in Table 3. The experimental compositions for the $V_2O_3(SO_4)_2$ electrodes were estimated based on the electrochemical data (Fig. 3(a)), assuming the oxidation states of lithium and oxygen were +1 and −2, respectively. The compositions of the chemically lithiated samples were obtained from ICP-OES analysis. The vanadium oxidation states of the lithiated samples are also given based on the compositions and the absorption edge energy, at half-height of the normalised XANES spectra.

In addition to using XANES analysis to confirm the change in vanadium oxidation state, IR spectra were collected. The IR spectra of $V_2O_3(SO_4)_2$, the $V_2O_3(SO_4)_2$ electrodes and the chemically lithiated phases are presented in Fig. 6(a) and (b), respectively. The IR spectrum of $V_2O_3(SO_4)_2$ exhibits absorption bands previously reported for $V_2O_3(SO_4)_2$, including the short vanadyl bond (993 cm^{-1}), intermediate V–O bond (948 cm^{-1}) and V–O–V bond (770 cm^{-1}).[23,37] It was expected that the

Open Access Article. Published on 10 September 2020. Downloaded on 12/6/2025 8:19:50 AM.
This article is licensed under a Creative Commons Attribution 3.0 Unported Licence.

Table 3 Summary of the experimental compositions of $Li_xV_2O_3(SO_4)_2$ materials and their vanadium oxidation states. The compositions of the electrochemically lithiated samples were estimated based on electrochemical data. The composition of the chemically lithiated samples were determined using ICP-OES analysis. The vanadium oxidation states are given based on the experimental compositions and the XANES data

Sample	Composition based on experimental data	Vanadium oxidation state based on composition	Edge energy/eV	Vanadium oxidation state based on edge energy
$V_2O_3(SO_4)_2$	$V_2O_3(SO_4)_2$	+5.00	5480.9(1)	+5.04(5)
Discharge 3.60 V	$Li_{0.39}V_2O_3(SO_4)_2$	+4.81	5479.8(1)	+4.48(5)
Discharge 2.95 V	$Li_{0.89}V_2O_3(SO_4)_2$	+4.57	5479.4(1)	+4.27(5)
Discharge 2.40 V	$Li_{1.40}V_2O_3(SO_4)_2$	+4.30	5478.8(1)	+3.87(5)
Discharge 1.95 V	$Li_{2.01}V_2O_3(SO_4)_2$	+3.99	5478.5(1)	+3.84(5)
Charge 4.00 V	$Li_{0.53}V_2O_3(SO_4)_2$	+4.74	5479.5(1)	+4.33(5)
1.46 mmol *n*BuLi	$Li_{0.97}V_2O_3(SO_4)_2$	+4.52(1)	5479.5(1)	+4.34(5)
2.92 mmol *n*BuLi	$Li_{1.64}V_2O_3(SO_4)_2$	+4.18(8)	5478.9(1)	+4.03(5)
5.85 mmol *n*BuLi	$Li_{2.47}V_2O_3(SO_4)_2$	+3.77(2)	5478.5(1)	+3.82(5)
11.70 mmol *n*BuLi	$Li_{3.97}V_2O_3(SO_4)_2$	+3.02(3)	5477.2(1)	+3.20(5)

vanadium oxidation state should decrease with increasing Li^+ content which is in agreement with the XANES analysis. As a result, one of the short V=O bonds of the $[VO_2]^+$ species and the V=O bond of the $[VO]^{3+}$unit should increase in length on insertion of 2.0 Li^+ which would form two $[VO]^{2+}$ species. On insertion of 4.0 Li^+, the $Li_{3.97}V_2O_3(SO_4)_2$ phase should not contain any short V=O bonds, as these are absent in V^{3+} phases.[38] The absorption band (993 cm^{-1}) corresponding to the short V=O bond shifts with varying Li^+ content.[23] Fig. 6(a) shows the V=O absorption band of $V_2O_3(SO_4)_2$ discharged to 3.50 V, 2.95 V, 2.40 V and 1.95 V shifts to lower frequencies of 983 cm^{-1}, 985 cm^{-1}, 975 cm^{-1} and 975 cm^{-1}, respectively, relative to $V_2O_3(SO_4)_2$ (993 cm^{-1}). While the V=O absorption band of the $V_2O_3(SO_4)_2$ electrode charged to 4.00 V shifted to a higher frequency 989 cm^{-1}, relative to the electrode discharged to 1.95 V (975 cm^{-1}). This shift suggests the V=O bond length increases with increasing Li^+ content and contracts on extraction of Li^+ which coincides with the XANES data.

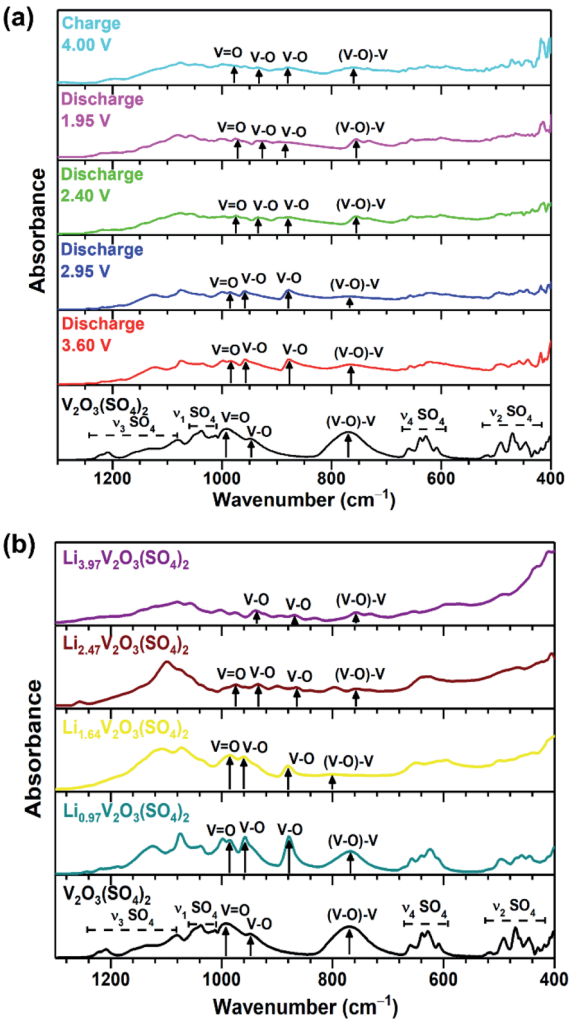

Fig. 6 IR spectra of (a) $V_2O_3(SO_4)_2$ (black) and the $V_2O_3(SO_4)_2$ electrode discharged to 3.60 V (red), discharged to 2.95 V (blue), discharged to 2.40 V (green), discharged to 1.95 V (pink), charged to 4.00 V (cyan) and (b) $Li_{0.97}V_2O_3(SO_4)_2$ (teal), $Li_{1.64}V_2O_3(SO_4)_2$ (yellow), $Li_{2.47}V_2O_3(SO_4)_2$ (maroon), $Li_{3.97}V_2O_3(SO_4)_2$ (purple).

Fig. 6(b) shows that V=O absorption band also shifts to lower frequencies of 985 cm^{-1}, 984 cm^{-1} and 975 cm^{-1} for $Li_{0.97}V_2O_3(SO_4)_2$, $Li_{1.64}V_2O_3(SO_4)_2$ and $Li_{2.47}V_2O_3(SO_4)_2$, respectively, demonstrating that the V=O bond length increases. In the case of $Li_{3.97}V_2O_3(SO_4)_2$, the intensity of the V=O bond almost disappears, suggesting that $Li_{3.97}V_2O_3(SO_4)_2$ does not contain the short vanadyl bond – consistent with a V^{3+} phase.[14,38]

Interestingly, the lithiated phases exhibit an additional absorption band at 880 cm^{-1}, not observed for $V_2O_3(SO_4)_2$. This band (880 cm^{-1}) is consistent with a longer V–O bond.[23,39,40] Its frequency suggests that it is longer than the other V–O bonds which exhibit absorption bands in the frequency range 934–960 cm^{-1}. This implies a change in the local structure around vanadium which will be discussed further in the subsequent section.

Structural evolution

To reveal the structural changes with Li^+ content, EXAFS analysis and PXRD studies were performed. Information on the changes in the local structure of the vanadium atoms was obtained by fitting the EXAFS data. A model based on the structure of the pristine phase, $V_2O_3(SO_4)_2$, was used to fit the EXAFS spectra. The local structure of vanadium in $V_2O_3(SO_4)_2$ is complex and the local environment of the V(1) and V(2) atoms is shown in Fig. 7.[24] Each vanadium atom is coordinated *via* six

 This journal is © The Royal Society of Chemistry 2020

Open Access Article. Published on 10 September 2020. Downloaded on 12/6/2025 8:19:50 AM.
This article is licensed under a Creative Commons Attribution 3.0 Unported Licence.

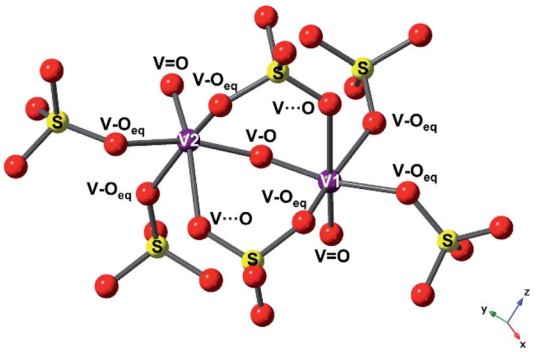

Fig. 7 Local environment of V(1) and V(2) atoms in $V_2O_3(SO_4)_2$, showing the different paths used in the EXAFS fitting model ((V═O) + (V–O) + (V–O_{eq}) + (V···O) + (V–O–S)), with the vanadium atoms shown as purple spheres, oxygen atoms as red spheres and sulfur atoms as yellow spheres.

V–O bonds (Table S2†). The vanadium atoms are both coordinated to a short terminal oxygen atom, V(1)═O(1) at 1.598(8) Å and V(2)═O(2) at 1.590(3) Å, and interconnected by a bridging oxygen atom, O(3), with V(1)═O(3) at 1.686(7) Å and V(2)–O(3) at an intermediate length of 1.781(4) Å, forming $[V(1)O_2]^+$ and $[V(2)O]^{3+}$. Each vanadium atom also shows three intermediate bonds, V–O_{eq} (~1.95(5) Å), and one long bond, V···O (~2.32(2) Å). Since the environments of V(1) and V(2) are similar, this structure was simplified into a five-path model consisting of a path for the short vanadyl bond (V═O), one for the short intermediate bond (V–O), one for the three equatorial bonds (V–O_{eq}), one for the long bond (V···O) and one for the V–O–S coordination, as illustrated in Fig. 7. During the fitting process, the atomic separations were refined, the coordination number (N) was held constant and one photoelectron energy shift (E_o) was fitted for the five paths. An amplitude reduction factor (S_o^2) of 1.0 was obtained by fitting the data from the pristine phase and used in the fitting of the data from lithiated materials. A different disorder factor (σ^2) for each path was used and fitting ranges of $4.0 < k < 13.0$ Å^{-1} and $1.0 < R < 4.0$ Å were employed. The fit values for E_o remained within ±10 eV. The experimental k^3-weighted EXAFS data fitted with the five-path model and the k^3-weighted Fourier Transform of the EXAFS for the electrochemically lithiated samples are shown in Fig. 8(a) and (b), respectively. The experimental k^3-weighted EXAFS data fitted with the five-path model and the k^3-weighted Fourier transform

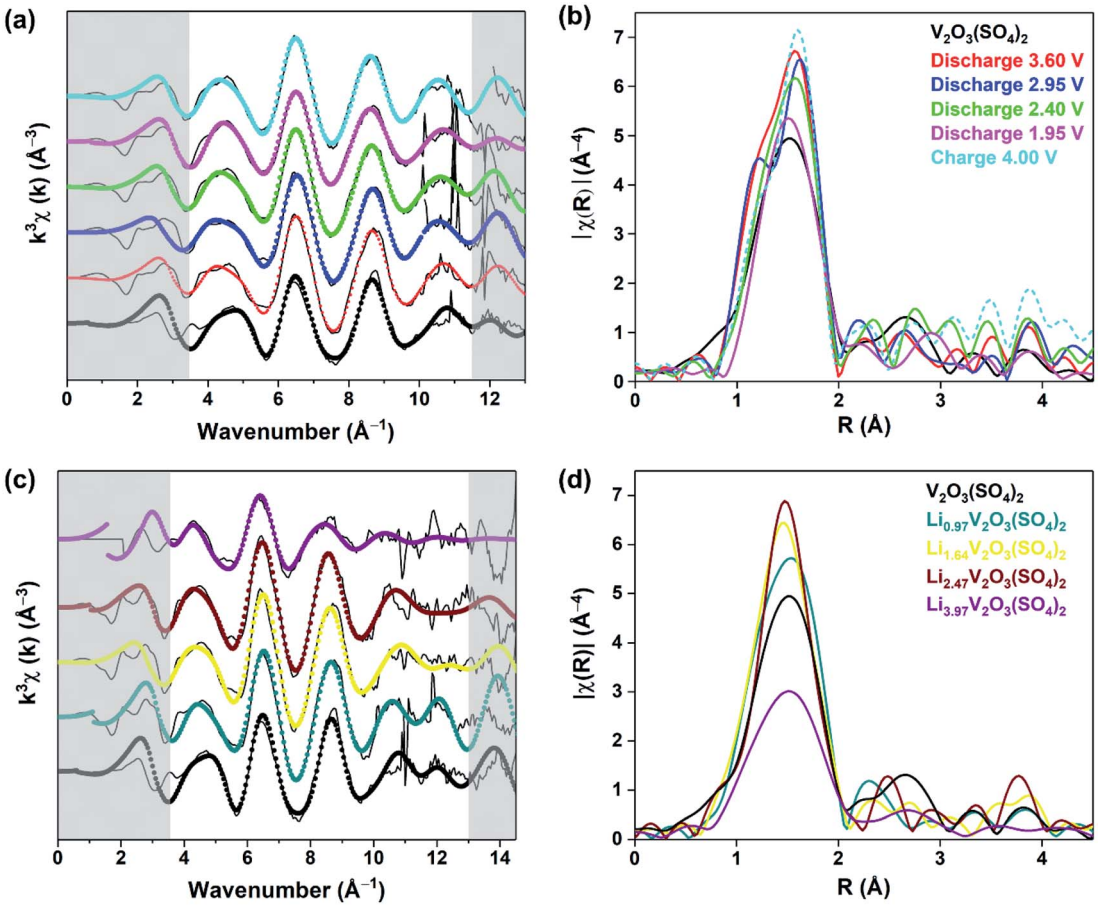

Fig. 8 (a) Experimental k^3-weighted EXAFS data (black lines) fitted with the five-path model (filled circles) and (b) their corresponding vanadium K-edge EXAFS spectra Fourier Transform in the R-space for the $V_2O_3(SO_4)_2$ electrode at various states of discharge and charge, (c) experimental k^3-weighted EXAFS data (black lines) fitted with the five-path model (filled circles) and (d) their corresponding vanadium K-edge EXAFS spectra Fourier Transform in the R-space for the chemically lithiated phases.

Open Access Article. Published on 10 September 2020. Downloaded on 12/6/2025 8:19:50 AM.
This article is licensed under a Creative Commons Attribution 3.0 Unported Licence.

of the EXAFS for the chemically lithiated samples are shown in Fig. 8(c) and (d), respectively. Note that the peaks of the k^3-weighted Fourier Transform have not been phase-shift corrected and appear at shorter distances than the atomic separations they represent.

Fig. 8(b) and (d) each show one distinct peak positioned in the 1–2 Å range, associated with the V–O local environment of the first coordination sphere with the majority of this peak originating from the three V–O_{eq} bonds.[32,33] The following peaks extending to 3.5 Å are dominated by contributions from the long V···O bond and the V–S single scattering paths. They show variations in the amplitude of the V–O contribution with Li^+ content, suggesting changes in the local arrangement of the first coordination sphere surrounding the vanadium atoms. Fig. 8(b) shows that the amplitude of the first peak increased after discharging to 3.60 V due to Li^+ insertion. The amplitude of this peak decreases on insertion of more Li^+ and increases again after extraction of Li^+.

The results from the fits of the EXAFS for the electrochemically lithiated samples are presented in Table S4.† The bond lengths for $V_2O_3(SO_4)_2$ are comparable to the bond lengths obtained from PXRD analysis (Table S2†). On cycling $V_2O_3(SO_4)_2$ *vs.* Li^+/Li^0, the V═O bond length fluctuated but remained within the range of a vanadyl bond (1.56(6)–1.60(4) Å).[38] This result was expected since the electrochemical data and XANES spectra both suggested that V^{5+} was reduced to V^{4+} which also contains a V═O bond.[38] The V–O bond, which models the bridging oxygen atom between to the two vanadium atoms increased in length to 1.83(5) Å after discharge to 1.95 V. This is consistent with a transition from V^{5+} to V^{4+} (*i.e.*, $[VO_2]^+$ to $[VO]^{2+}$) on insertion of 2.0 Li^+ per mol of $V_2O_3(SO_4)_2$. On extraction of Li^+, the V–O bond contracted again to 1.78(1) Å consistent with a $[VO]^{2+}$ to $[VO_2]^+$ transition, in agreement with the XANES data. Fig. 8(d) shows an increase in the amplitude of the first peak with increasing Li^+ content which can be attributed to a higher degree of symmetry surrounding the vanadium atoms with increasing Li^+ content.[32,33]

However, in the case of the $Li_{3.97}V_2O_3(SO_4)_2$ phase, the intensity of the V–O contribution decreased significantly. Since the symmetry surrounding the vanadium atoms continued to increase with increasing Li^+, this effect was probably outweighed by an increase in the disorder as the V–O bonds became longer and weaker. Fig. 8(c) shows the spectrum of $Li_{3.97}V_2O_3(SO_4)_2$ is noisy, with no signal beyond 11 $Å^{-1}$ so the k-range was restricted to $3.6 < k < 10.8$ $Å^{-1}$ and $1.0 < R < 4.0$ Å. However, with this range the five-shell model gave nonsensical parameters, including either negative or extremely large disorder factors and E_o values greater than 10 eV. Consequently, other models were tested. A satisfactory fit was obtained with a four-path model consisting of a path for the two short vanadyl bonds (V═O), one for the three equatorial bonds (V–O_{eq}), one for the long bond (V···O) and one for the V–O–S coordination. The fitting parameters show an increase in the V–O bond lengths compared to the other samples. The short V═O bond distance (1.67(2) Å) increased in length by 0.07 Å compared to the pristine phase and is midway between the V═O and V–O–V bond.

The equatorial bonds (V–O_{eq}) also increased in length (2.04(4) Å) and are consistent with V^{3+}–O bond lengths.[41] These results are broadly consistent with the reduction of V^{5+} to V^{3+}, since longer and weaker bonds were obtained from this analysis. Additionally, there is more disorder associated with the V–O bonds of $Li_{3.97}V_2O_3(SO_4)_2$ which is also consistent with V^{3+}–O bonds. Moreover, there is a correlation between the intensity of the pre-edge peak of the XANES spectrum and the size of the VO_x coordination sphere.[31] The reduced intensity of the pre-edge peak of $Li_{3.97}V_2O_3(SO_4)_2$ relative to the other phases is consistent with the disappearance of the V═O bond. This observation is consistent with the IR spectrum for this phase, suggesting $Li_{3.97}V_2O_3(SO_4)_2$ consists of more regular VO_6 octahedra compared to the distorted VO_6 octahedra of $V_2O_3(SO_4)_2$.

To follow the long-range structural changes, PXRD patterns of the lithiated phases were collected. Fig. 9(a) compares the PXRD patterns of the electrochemically lithiated samples and Fig. 9(b) compares the PXRD patterns of the chemically lithiated samples. The lithiated materials show no additional reflections compared to $V_2O_3(SO_4)_2$, implying no secondary phases were formed on Li^+ insertion. Fig. 9 reveals a shift of the reflections for the lithiated samples relative to $V_2O_3(SO_4)_2$, suggesting the unit cell volume changed on Li^+ insertion. It can be assumed that the lithiated materials retained the monoclinic symmetry of $V_2O_3(SO_4)_2$ since the PXRD patterns of $V_2O_3(SO_4)_2$ and the lithiated phases are similar.

To establish the changes in the unit cell parameters, a series of Rietveld refinements were performed using the structural model of $V_2O_3(SO_4)_2$ as the starting model.[24] The same general procedure was followed for each refinement, the backgrounds were fitted using a Chebyshev polynomial with 36 terms, the unit cell parameters, zero-error and profile parameters were all refined. Good fits were obtained and the fits between 9–12° 2θ are presented in Fig. S3(a–j),† highlighting the shifts of the reflections relative to the pristine phase. The corresponding changes in the unit cell parameters are given in Table S3.† The relationship between the Li content (x Li in $Li_xV_2O_3(SO_4)_2$) and the unit cell volume for the electrochemically lithiated samples is illustrated in Fig. 9(c). This shows there was an expansion of the unit cell volume of roughly 3.5% on insertion of 0.39 mol Li^+ after discharging to 3.60 V. This can be explained by the size-expansion of the VO_6 octahedra due to the partial reduction of V^{5+} to V^{4+} and the insertion of Li^+.[42] Inserting more Li^+ caused the unit cell volume to contract. This can be rationalised by the increased electrostatic attraction with increasing Li^+ content which outweighed the size-expansion of the VO_6 octahedra due to the reduction of V^{5+} to V^{4+}. If 1.0 Li^+ was inserted into $V_2O_3(SO_4)_2$, according to the linear relationship shown in Fig. 9(c), $LiV_2O_3(SO_4)_2$ would have a unit cell volume of 836(1) $Å^3$. This corresponds to a 3.1(1)% volume expansion relative to the pristine phase. This volume change is comparable with volume changes reported in the literature for other vanadium-based polyanionic electrode materials.[13,14,18]

The evolution of the unit cell volume after chemical lithiation is presented in Fig. 9(d). This shows the relationship between the Li^+ content (xLi in $Li_xV_2O_3(SO_4)_2$) obtained from ICP-OES analysis and the unit cell volume obtained from the

 This journal is © The Royal Society of Chemistry 2020

Open Access Article. Published on 10 September 2020. Downloaded on 12/6/2025 8:19:50 AM.
This article is licensed under a Creative Commons Attribution 3.0 Unported Licence.

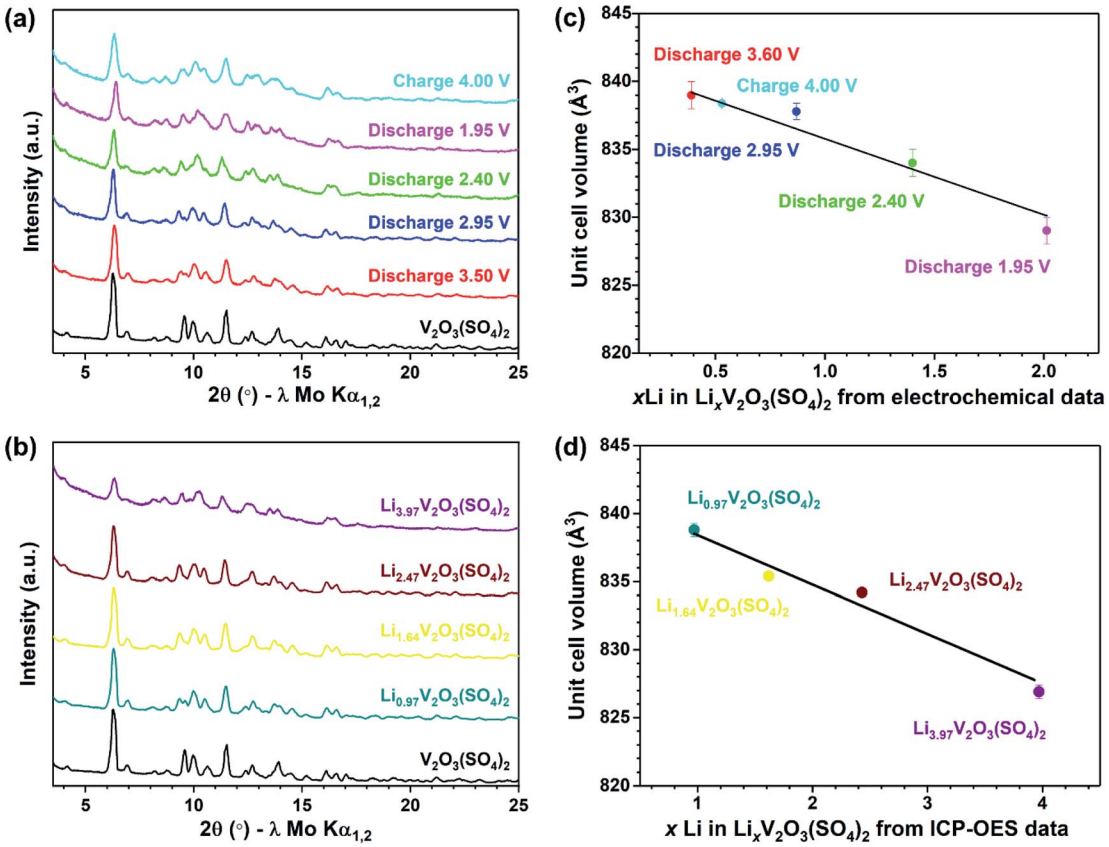

Fig. 9 (a) PXRD patterns of $V_2O_3(SO_4)_2$ (black), $V_2O_3(SO_4)_2$ electrode discharged to 3.50 V (red), discharged to 2.95 V (blue), discharged to 2.40 V (green), discharged to 1.95 V (pink), charged to 4.00 V (cyan), (b) PXRD patterns of the chemically lithiated phases, $Li_{0.97}V_2O_3(SO_4)_2$ (teal), $Li_{1.64}V_2O_3(SO_4)_2$ (yellow), $Li_{2.47}V_2O_3(SO_4)_2$ (maroon) and $Li_{3.97}V_2O_3(SO_4)_2$ (purple), (c) the effect of xLi in $Li_xV_2O_3(SO_4)_2$ based on electrochemical data on the unit cell volume of electrochemically lithiated materials and (d) the effect of xLi in $Li_xV_2O_3(SO_4)_2$ as determined from ICP-OES analysis on the unit cell volume of chemically lithiated materials.

Rietveld refinements. Fig. 9(d) shows the unit cell volume decreased linearly with increasing Li^+ content. This result coincides with the change in unit cell volume observed for the electrochemically lithiated materials, demonstrating that the structural changes during the electrochemical lithiation were replicated chemically.

Conclusions

This work has investigated for the first time the Li^+ insertion process into $V_2O_3(SO_4)_2$ *via* electrochemical and chemical routes. $V_2O_3(SO_4)_2$ delivers an initial discharge capacity of approximately 160 mA h g^{-1}, corresponding to the insertion of approximately 2.0 Li^+ per formula unit, associated with four redox processes at 4.09 V, 3.25 V, 2.83 V and 2.23 V attributed to the V^{4+}/V^{5+} redox couple. XANES measurements of the electrochemically lithiated materials showed that 2.0 Li^+ ions were incorporated to give $Li_2V_2O_3(SO_4)_2$. As for the chemically lithiated materials, ICP-OES data and XANES measurements revealed that up to 4.0 Li^+ ions can be inserted into $V_2O_3(SO_4)_2$, reducing V^{5+} to V^{3+}. Structural studies by PXRD revealed that the monoclinic symmetry of $V_2O_3(SO_4)_2$ was retained with Li^+ insertion and was accompanied by changes in the unit cell volume. This analysis showed that the structural transformation which occurred during electrochemical lithiation was replicated chemically and that 4.0 Li^+ ions can be inserted into $V_2O_3(SO_4)_2$ while it maintained its framework structure.

This material exploits the property of vanadium to adopt numerous oxidation states and offers structural stability. This highlights the potential of vanadium sulfates and the opportunities to explore new vanadium-based polyanionic compounds.

Conflicts of interest

There are no conflicts to declare.

Acknowledgements

The authors thank M. Nowosielska for ICP-OES measurements. The authors are grateful for the provision of beam time and assistance from Dr Giannantonio Cibin on B18 at the Diamond Light Source (as part of the Energy Materials Block Allocation Group SP14239) and Dr Ron Smith on the GEM diffractometer at ISIS Neutron and Muon Source at the Rutherford Appleton

Laboratory. The authors also thank EPSRC for funding of SFL's PhD thesis (EP/N509759/1).

References

1 M. S. Whittingham, *Chem. Rev.*, 2004, **104**, 4271–4301.
2 A. Manthiram and J. B. Goodenough, *J. Power Sources*, 1989, **26**, 403–408.
3 C. Masquelier and L. Croguennec, *Chem. Rev.*, 2013, **113**, 6552–6591.
4 Y. Wang, Y. Wang, E. Hosono, K. Wang and H. Zhou, *Angew. Chem., Int. Ed.*, 2008, **47**, 7461–7465.
5 J. Wang and X. Sun, *Energy Environ. Sci.*, 2012, **5**, 5163–5185.
6 P. Barpanda, M. Ati, B. C. Melot, G. Rousse, J.-N. Chotard, M.-L. Doublet, M. T. Sougrati, S. A. Corr, J.-C. Jumas and J.-M. Tarascon, *Nat. Mater.*, 2011, **10**, 772–779.
7 M. Kim, Y. Jung and B. Kang, *J. Mater. Chem. A*, 2015, **3**, 7583–7590.
8 R. K. B. Gover, P. Burns, A. Bryan, M. Y. Saidi, J. L. Swoyer and J. Barker, *Solid State Ionics*, 2006, **177**, 2635–2638.
9 J. Barker, R. K. B. Gover, P. Burns, A. Bryan, M. Y. Saidi and J. L. Swoyer, *J. Power Sources*, 2005, **146**, 516–520.
10 J. Barker, R. K. B. Gover, P. Burns, A. Bryan, M. Y. Saidi and J. L. Swoyer, *J. Electrochem. Soc.*, 2005, **152**, A1776–A1779.
11 J. Barker, R. K. B. Gover, P. Burns and A. Bryan, *Electrochem. Solid-State Lett.*, 2005, **8**, A285–A287.
12 J.-M. Ateba Mba, C. Masquelier, E. Suard and L. Croguennec, *Chem. Mater.*, 2012, **24**, 1223–1234.
13 M. Bianchini, J. M. Ateba-Mba, P. Dagault, E. Bogdan, D. Carlier, E. Suard, C. Masquelier and L. Croguennec, *J. Mater. Chem. A*, 2014, **2**, 10182–10192.
14 K. L. Harrison, C. A. Bridges, C. U. Segre, C. D. V. Jr, D. Applestone, C. W. Bielawski, M. P. Paranthaman and A. Manthiram, *Chem. Mater.*, 2014, **26**, 3849–3861.
15 J. Barker, M. Y. Saidi and J. L. Swoyer, *J. Electrochem. Soc.*, 2004, **151**, A796–A800.
16 M. S. Kishore, V. Pralong, V. Caignaert, U. V. Varadaraju and B. Raveau, *Electrochem. Commun.*, 2006, **8**, 1558–1562.
17 M. Satya Kishore, V. Pralong, V. Caignaert, S. Malo, S. Hebert, U. V. Varadaraju and B. Raveau, *J. Solid State Chem.*, 2008, **181**, 976–982.
18 M. Sun, G. Rousse, M. Saubanère, M.-L. Doublet, D. Dalla Corte and J.-M. Tarascon, *Chem. Mater.*, 2016, **28**, 6637–6643.
19 J. Gaubicher, Y. Chabre, J. Angenault, A. Lautié and M. Quarton, *J. Alloys Compd.*, 1997, **262–263**, 34–38.
20 K. S. Nanjundaswamya, H. Araib, J. Yamakib, S. Okadab and H. Ohtsukab, *Solid State Ionics*, 1996, **92**, 1–10.
21 J. Gaubicher, J. Angenaut, Y. Chabre, T. Le Mercier and M. Quarton, *Mol. Cryst. Liq. Cryst.*, 1998, **311**, 45–50.
22 L. Lander, J.-M. Tarascon and A. Yamada, *Chem. Rec.*, 2018, **18**, 1394–1408.
23 K.-L. Richter and R. Mattes, *Z. Anorg. Allg. Chem.*, 1992, **611**, 158–164.
24 B. H. Toby, *J. Appl. Crystallogr.*, 2001, **34**, 210–213.
25 A. C. Larson and R. B. Von Dreele, *GSAS - General Structure Analysis System, LANL Report*, Los Alamos National Laboratory, LAUR, Los Alamos, USA, 2001, pp. 86–748.
26 B. Ravel and M. Newville, *Phys. Scr.*, 2005, **115**, 1007–1010.
27 B. Ravel and M. Newville, *J. Synchrotron Radiat.*, 2005, **12**, 537–541.
28 T. Ohzuku, J. Kato, K. Sawai and T. Hirai, *J. Electrochem. Soc.*, 1991, **138**, 2556–2560.
29 H. Björk, T. Gustafsson, J. O. Thomas, S. Lidin and V. Petříček, *J. Mater. Chem.*, 2003, **13**, 585–589.
30 Y. J. Lee, F. Wang, S. Mukerjee, J. McBreen and C. P. Grey, *J. Electrochem. Soc.*, 2000, **147**, 803–812.
31 J. Wong, F. W. Lytle, R. P. Messmer and D. H. Maylotte, *Phys. Rev. B: Condens. Matter Mater. Phys.*, 1984, **30**, 5596–5610.
32 C. J. Allen, Q. Jia, C. N. Chinnasamy, S. Mukerjee and K. M. Abraham, *J. Electrochem. Soc.*, 2011, **158**, 1250–1259.
33 A. N. Mansour, P. H. Smith, W. M. Baker, M. Balasubramanian and J. McBreen, *Electrochim. Acta*, 2002, **47**, 3151–3161.
34 T. Tsunehiro, Y. Hiromi, T. Risa, F. Takuzo and Y. Satohiro, *J. Chem. Soc.*, 1988, **84**, 2987–2999.
35 G. A. Horrocks, E. J. Braham, Y. Liang, L. R. De Jesus, J. Jude, J. M. Velázquez, D. Prendergast and S. Banerjee, *J. Phys. Chem. C*, 2016, **120**, 23922–23932.
36 Y. U. Park, D. H. Seo, H. S. Kwon, B. Kim, J. Kim, H. Kim, I. Kim, H. I. Yoo and K. Kang, *J. Am. Chem. Soc.*, 2013, **135**, 13870–13878.
37 A. P. Tyutyunnik, V. N. Krasil, V. G. Zubkov, L. A. Perelyaeva and I. V Baklanova, *Russ. J. Inorg. Chem.*, 2010, **55**, 554–560.
38 M. Schindler, F. C. Hawthorne and W. H. Baur, *Chem. Mater.*, 2000, **12**, 1248–1259.
39 A. P. Tyutyunnik, V. G. Zubkov, I. F. Berger, V. N. Krasil, L. A. Perelyaeva and I. V Baklanova, *Russ. J. Inorg. Chem.*, 2007, **52**, 1521–1526.
40 V. N. Krasil'nikov, A. P. Tyutyunnik, L. A. Perelyaeva and I. V Baklanova, *Russ. J. Inorg. Chem.*, 2013, **58**, 161–167.
41 J. Krakowiak, D. Lundberg and I. Persson, *J. Inorg. Chem.*, 2012, **51**, 9598–9609.
42 R. D. Shannon, *Acta Crystallogr., Sect. A: Cryst. Phys., Diffr., Theor. Gen. Crystallogr.*, 1976, **32**, 751–767.

Open Access Article. Published on 10 September 2020. Downloaded on 12/6/2025 8:19:50 AM.
This article is licensed under a Creative Commons Attribution 3.0 Unported Licence.

This journal is © The Royal Society of Chemistry 2020